Supplementary Material

Seung Ju Yoon, Da In Song, Jungmin Lee, Myung-Ki Kim, Yong-Hee Lee* and Chang-Kyu Kim*

***Corresponding author: Chang-Kyu Kim**, Department of Nano & Semiconductor Engineering, Korea Polytechnic University, Siheung 15073, South Korea, e-mail: ckkim@kpu.ac.kr

***Corresponding author: Yong-Hee Lee,** Department of Physics, Korea Advanced Institute of Science and Technology (KAIST), Daejeon 34141, South Korea, e-mail: yhlee@kaist.ac.kr

Seung Ju Yoon, Da In Song, Jungmin Lee, Department of Physics, Korea Advanced Institute of Science and Technology (KAIST), Daejeon 34141, South Korea

Myung-Ki Kim, KU-KIST Graduate School of Converging Science and Technology, Korea University, Seoul 02841, South Korea

Hopping of Single Nanoparticles Trapped in a Plasmonic Double-Well Potential

S1 Fabrication of a three-dimensional tapered plasmonic nanoantenna

The three-dimensional (3D) tapered metallic cavity used in this study was bow-tie shaped; two protrusions separated by a nanoscale gap tapered toward the bottom plane, as shown in Figure 1A. A 100-nm-thick gold film was sputtered on a fused quartz substrate at an evaporation rate of 0.5 $Å s^{-1}$ without an adhesion layer. To fabricate the nanoscale metal gap, we intentionally separated two triangle milling patterns to utilize the proximity effect of a Ga^{+}-based focused ion beam milling (model: Helios NanoLab FEI) (Figure S1A). By changing the distance (*s*) between the two triangular milling patterns, we could fabricate gaps smaller than 10 nm. The scanning electron microscope (SEM) images for gap sizes 0–10 nm are shown in Figure S1B. The length (*L*) and width (*W*) of the antenna were 200 and 160 nm, respectively, and the vertical taper angle was measured to be approximately 65°. The spacing between the metal tips was measured by counting the number of pixels in the SEM image taken at 52°. When the fabricated nanogap was smaller than the resolution of the SEM (< 5 nm), two tips appeared to be connected owing to the scattering of the SEM electron beam. However, the optical pumping produced a bright second harmonic (SH) signal in the disconnected tips, but not in the connected ones.

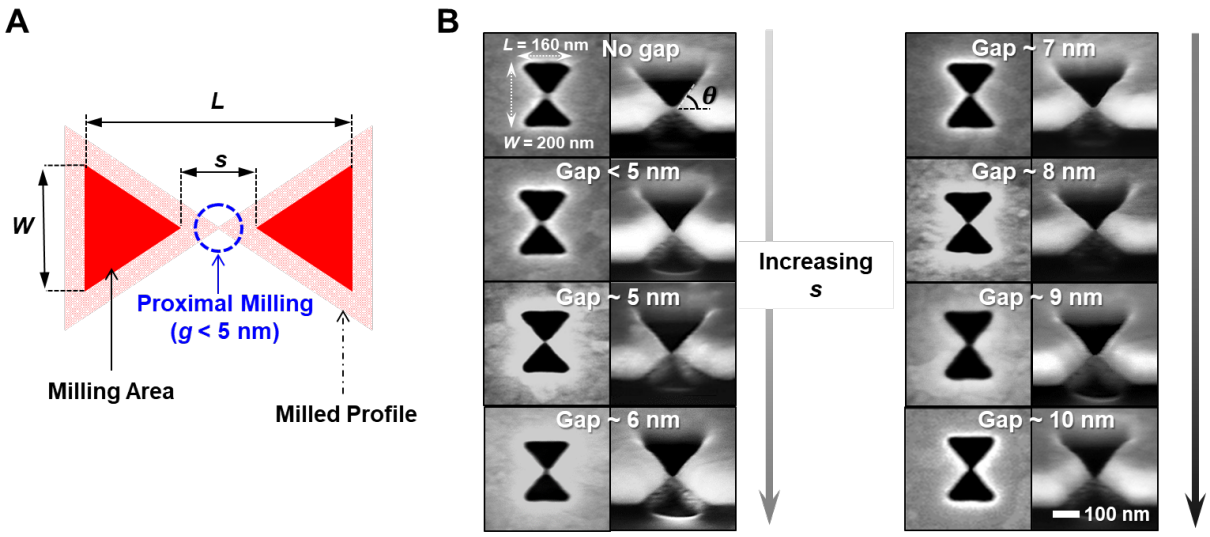

Figure S1: Fabrication of a 3D plasmonic nanoantenna. (A) Schematic of the proximal technique in the focused ion beam milling process. (B) Scanning electron microscope images of top and 52°-tilted views of the fabricated 3D plasmonic nanoantennas with different distance (*s*). As *s* changed, the gap size in the nanoantenna increased from 0 nm (the attached structure) to 10 nm. The images are in the increasing order of gap sizes.

S2 Optical potential with various continuous-wave laser power

The optical potential profile and induced force applied to a 4-nm-diameter CdSe/ZnS quantum dot (QD) were calculated by using Maxwell stress tensor (MST).

The Lorentz force per unit volumes is

$$\mathbf{f} = \rho\mathbf{E} + \mathbf{J} \times \mathbf{B}, \qquad \text{(S1)}$$

where ρ is the total charge per unit volume, $\mathbf{E}$ is the electric field, $\mathbf{J}$ is the total current density, and $\mathbf{B}$ is the magnetic field. Using Gauss's law and Ampere's circuital law,

$$\nabla \cdot \mathbf{E} = \frac{\rho}{\varepsilon}, \nabla \times \mathbf{B} = \mu\mathbf{J} + \mu\varepsilon\frac{\partial \mathbf{E}}{\partial t}, \qquad \text{(S2)}$$

ρ and $\mathbf{J}$ can be replaced by the electric and magnetic field,

$$\mathbf{f} = \varepsilon(\nabla \cdot \mathbf{E})\mathbf{E} + \frac{1}{\mu}(\nabla \times \mathbf{B}) \times \mathbf{B} - \varepsilon\frac{\partial \mathbf{E}}{\partial t} \times \boldsymbol{B}$$

$$= \varepsilon\left[(\nabla \cdot \mathbf{E})\mathbf{E} + (\mathbf{E} \cdot \nabla)\mathbf{E} - \frac{\mathbf{1}}{\mathbf{2}}\nabla E^2\right] + \frac{1}{\mu}\left[(\nabla \cdot \mathbf{B})\mathbf{B} + (\mathbf{B} \cdot \nabla)\mathbf{B} - \frac{\mathbf{1}}{\mathbf{2}}\nabla B^2\right] - \varepsilon\frac{\partial}{\partial t}(\mathbf{E} \times \mathbf{B}). \quad \text{(S3)}$$

By introducing the MST,

$$\overleftrightarrow{\boldsymbol{T}}_{ij} = \varepsilon\left(\mathrm{E}_i\mathrm{E}_j - \frac{1}{2}\delta_{ij}E^2\right) + \frac{1}{\mu}\left(\mathrm{B}_i\mathrm{B}_j - \frac{1}{2}\delta_{ij}B^2\right), \quad \text{(S4)}$$

the time-averaged force becomes

$$\langle\mathbf{f}\rangle_{time-averaged} = \langle\nabla \cdot \mathbf{T}\rangle_{time-averaged}, \qquad \text{(S5)}$$

where the last term of $\mathbf{f}$ vanishes via time averaging. The total force on a QD is calculated as a volume integral,

$$\mathbf{F} = \int_v \mathbf{f}\,\mathrm{d}\tau = \int_v \nabla \cdot \mathbf{T}\,\mathrm{d}\tau. \qquad \text{(S6)}$$

Then, the optical potential is obtained by integrating the total force along the path from a reference point where the potential energy is considered to be zero.

$$\mathbf{U} = -\int_{\boldsymbol{ref}}^{\boldsymbol{r}} \vec{\mathbf{F}} \cdot \mathrm{d}\vec{\boldsymbol{r}}. \quad \text{(S7)}$$

The electromagnetic field distribution was computed using the finite-difference time-domain (FDTD) simulation. A triple mesh structure was adapted considering the simulation accuracy and time. The whole FDTD computational domain was defined as a cuboid volume of 2,000 × 2,000 × 1,000 nm^3 divided by uniformly partitioned 6-nm spatial grids. An additional 0.5 × 0.5 × 0.5 nm^3 mesh was used in a 300 × 200 × 150 nm^3 volume, which was larger than the size of the antenna.

Finally, $0.1 \times 0.1 \times 0.1$ nm^3 mesh was imposed in a $20 \times 20 \times 10$ nm^3 volume containing the central gap.

The optically induced potential along the *y*-direction of a 5-nm-gap plasmonic antenna on a 4-nm-diameter CdSe/ZnS QD was calculated for the incident pump power of 10 mW. Here, the *y*-axis position was defined as the center-of-mass coordinate of the QD projected onto the *y*-axis when it moved along the slope. As the incident continuous-wave (CW) laser power increased, the depth of the well, oscillation frequency at the bottom of the well, oscillation frequency at the top of the barrier, and central barrier height linearly increased, as shown in Figure S2. The change rates of the essential parameters for various gap sizes are listed in Table 1.

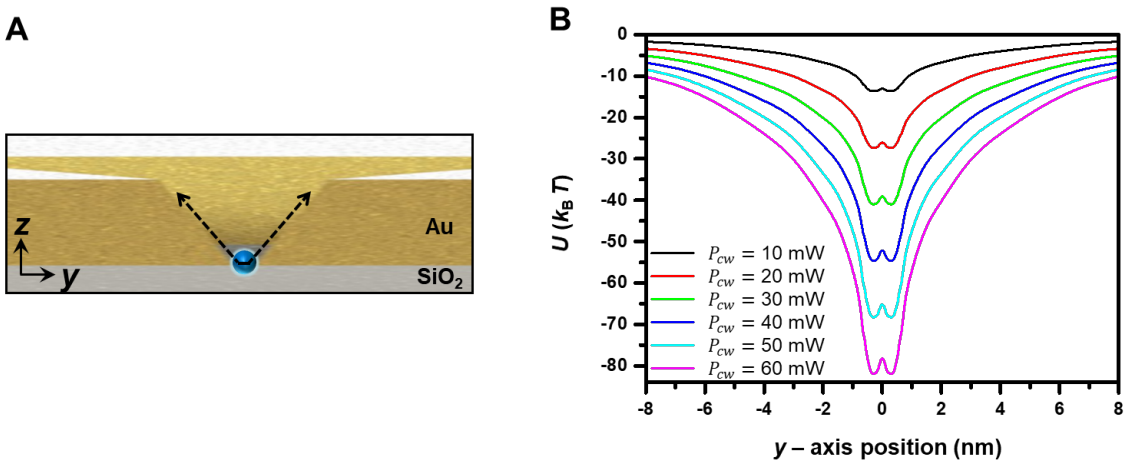

Figure S2: Double-well potential profile as a function of incident pump power for 5-nm-gap plasmonic nanoantenna. (A) The motion of a QD inside a plasmonic nanoantenna. (b) The optical potential (U) was calculated for a 4-nm-diameter QD moving along *y*-axis with incident powers (P_{CW}) from 10 mW (black line) to 60 mW (purple line).

S3 Brownian motion in a potential well

The potential profile along the *x*- and *z*-directions of the nanoantenna has been presented in a previous work for a single-well [1]. For an order-of-magnitude estimation of the oscillation frequency in water, we considered the theoretical roll-off frequency of a free sphere. In an overdamped trapping system, the power spectrum of Brownian motion in a harmonic potential can be described as a Lorentzian function, and the roll-off frequency is given by $f_c = \alpha/(2\pi\beta)$, where α is the trap stiffness and β is the drag coefficient on the particle [2]. α can be derived from the equipartition theorem, $\frac{1}{2}\alpha < d >^2 = \frac{1}{2}k_B T$, where d is the displacement of the particle from its equilibrium position, k_B is the Boltzmann constant, and T is the absolute temperature.

For a 5-nm-gap plasmonic nanoantenna, we set d = 5 and 7 nm for the *x*- and *z*-directions because the oscillation width of the trapped particle was assumed to be comparable to the dimension of the mode volume, 5 × 5 × 7 nm^3. For a QD in water, the roll-off frequency (f_c) was approximately 5 and 2.5 MHz in the *x*- and *z*-direction potential well, respectively. This order of magnitude was significantly higher than the hopping rate (ca. 10 Hz) observed in this study, even considering the wall effect. (Supplementary Material S4)

S4 Kramers transition equation

By using a multiplicative bridging version of Kramers formula, which is composed of a high damping equation (r^{HF}) and a low damping equation (r^{LF}), the transition rate (f_c^{Theory}) can be calculated for a wide range of damping regimes (equation S8-S11) [3-8].

$$f_c^{Theory} = \frac{\pi}{\omega_0} r^{LF} r^{HF} exp\left(\frac{U_b}{k_B T}\right), \qquad (S8)$$

$$r^{\mathrm{LF}} = \frac{\omega_0}{\pi} exp\left[\frac{1}{\pi}\int_0^{\infty} \frac{ln\left\{1-exp\left[-\Delta\left(x^2+\frac{1}{4}\right)\right]\right\}}{\left(x^2+\frac{1}{4}\right)} dx\right] exp\left(-\frac{U_\mathrm{b}}{k_\mathrm{B}T}\right), \quad \text{(S9)}$$

$$\Delta = \frac{\gamma}{k_\mathrm{B}T}\int_{-\frac{c}{2}}^{\frac{c}{2}} \sqrt{2m[U_\mathrm{b} - U(y)]}\, dy, \text{ and} \quad \text{(S10)}$$

$$r^{\mathrm{HF}} = \frac{\omega_0}{\pi}\left(\sqrt{\frac{\gamma^2}{4\omega_\mathrm{b}^2}+1} - \frac{\gamma}{2\omega_\mathrm{b}}\right) exp\left(-\frac{U_\mathrm{b}}{k_\mathrm{B}T}\right), \quad \text{(S11)}$$

where $\omega_0 = \sqrt{V''(x)/m}$ is the oscillation frequency near the bottom of the well, ω_b is the oscillation frequency at the top of the barrier, U_b is the height of the energy barrier, k_B is the Boltzmann constant, T is the temperature (300 K), Δ is the action of a particle from the minimum of the potential well to the energy barrier, γ is the damping coefficient of the surrounding environment, c is the distance between two wells, and m is the mass of the particle.

In our optical trapping system, a QD is trapped in a dilute aqueous solution at room temperature and atmospheric pressure. The damping coefficient γ in this system is calculated by using the relation $\gamma = 6\pi\eta a/M_{\mathrm{QD}}$, where η is the viscosity of water, and a is the QD radius. Our trapping system corresponds to a high-damping regime with a large damping coefficient ($\gamma \sim 1\times10^{11}\ \mathrm{s}^{-1} >> \omega_0, \omega_\mathrm{b}$), and the exponential term with integral of r^{LF} in Equation S9 converges to 1. The Kramers formula can be approximated by a Taylor expansion and described by

$$f_\mathrm{c} \approx \left(\frac{\omega_0}{\pi}\right)\left(\frac{\omega_\mathrm{b}}{\gamma}\right) exp\left(-\frac{U_\mathrm{b}}{k_\mathrm{B}T}\right). \quad \text{(S12)}$$

The hopping rate is critically determined by the height of the energy barrier and the oscillation frequency, which are ratios of the trap stiffness α and Stokes' drag coefficient β_0 in free space.

For a particle moving near a rigid wall, a nearby surface increases the hydrodynamic force, and the Stokes' drag coefficient is modified by multiplying a wall correction factor F [9-11]

$$\beta' = F \times \beta_0. \quad \text{(S13)}$$

Thus, the motion of the particle near the wall is expressed by

$$\omega' = \frac{\alpha}{\beta'} = \frac{\alpha}{F \times \beta_0} = \frac{\omega}{F}. \quad \text{(S14)}$$

Here, F is determined by the geometry of the wall, radius of the particle, and distance from the center of the particle to the wall. Since the QD moves near the wall, the oscillation frequencies in Equation S12 are replaced by ω_0' and ω_b'. Therefore,

$$f_c' \cong \left(\frac{\omega_0'}{\pi}\right)\left(\frac{\omega_b'}{\gamma}\right) exp\left(-\frac{U_b}{k_B T}\right)$$

$$= \left(\frac{1}{F^2}\right)\left(\frac{\omega_0}{\pi}\right)\left(\frac{\omega_b}{\gamma}\right) exp\left(-\frac{U_b}{k_B T}\right). \quad \text{(S15)}$$

From Equation S12 and Equation S15,

$$f_c' = \frac{1}{F^2} f_c. \quad \text{(S16)}$$

Thus the hopping rate is reduced by $1/F^2$. In our experiment, F was estimated to be 3–100.

S5 Optical measurement setup

We used a confocal optical setup that included a CW laser (Thorlabs, Product No. FPL1009S, λ = 1560 nm) and a femtosecond laser (Toptica FemtoFiber pro NIR, λ= 1560 nm, 100-fs pulse, 80 MHz) as shown in Figure S3. The CW laser with an incident power of 10 mW (0.3 MW cm^{-2}) to

70 mW (2.1 MW cm^{-2}) was used as a trapping laser to build an optical potential. The femtosecond-pulsed laser with a peak power of approximately 12.5 GW cm^{-2} was used as a probe laser for generating the SH signal at the tips of the antennas. The two laser beams were combined using a 25:75 (Femtosecond:CW) beam coupler and filtered with a long-pass filter ($\lambda_{cut\text{-}off}$ = 1.2 μm). They were polarized along the transverse direction (*y*-axis in Figure 1) and focused onto the sample by a microscope objective lens (Newport, Model: 5721-C-H, 60×, Numerical Aperture 0.65). After supplying CdSe/ZnS QDs (Nanosquare, Product No. C01-SH01-AC-100620, $\lambda_{emission}$: ca. 620 nm, diameter: ca. 4 nm), light signals from the sample were collected from the top side through a microscope objective lens (Olympus, Model: LUCPlanFL N, 60×, 075 NA). The transmitted signal of both the CW and femtosecond lasers was separated by a beam splitter and recorded using an infrared photodiode (Femtowatt InGaAs Photo-receiver, Newport, Model: 2153). The SH signal was monitored by a visible electron-multiplying charge-coupled device (Andor technology, iXon3 897), after passing passed through a short-pass filter ($\lambda_{cut\text{-}off}$ = 1.3 μm) and a band-pass filter (λ_{center} = 780 ± 10 nm). Both signals were recorded simultaneously in real time.

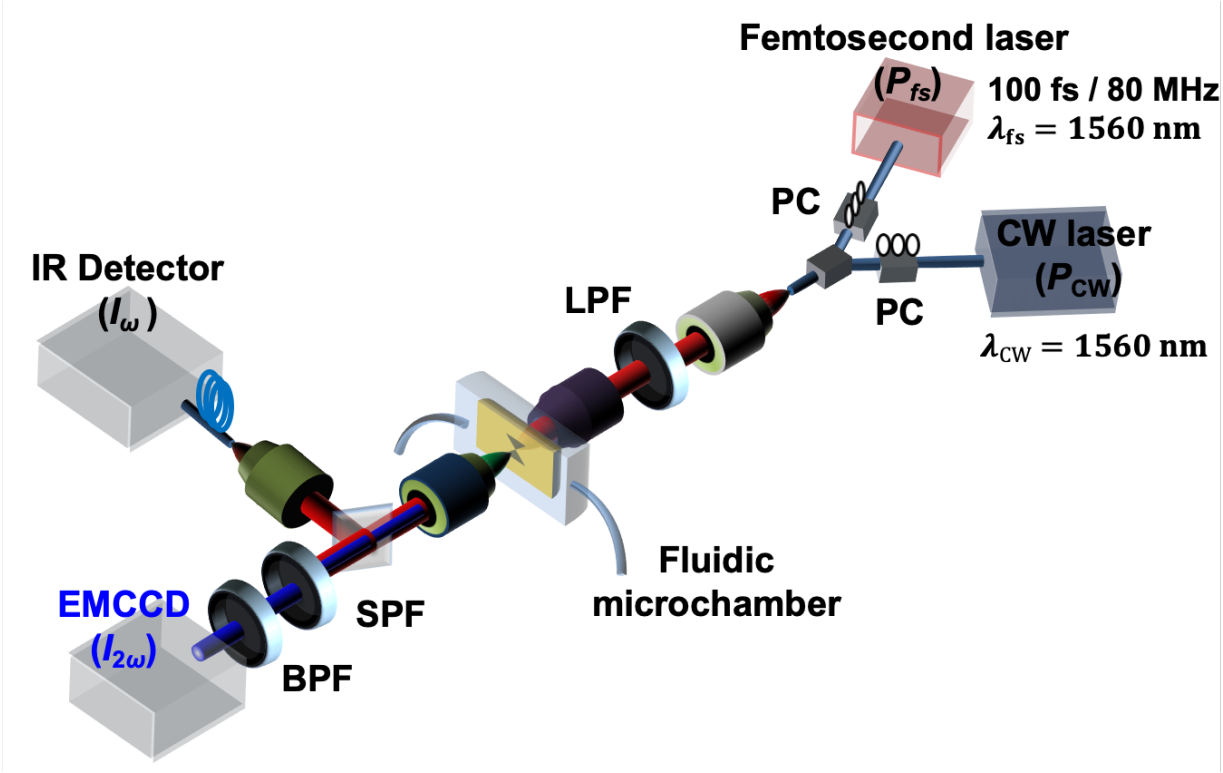

Figure S3: Two-laser system. Both laser beams were polarized using polarization controllers (PCs) and combined using a 25:75 (Femtosecond:CW) coupler. The beam passed through a long-pass filter (LPF) and was focused on the antenna with a 60× objective lens. The transmitted pump signal (I_ω) was monitored by an infrared photodetector (IR Detector). The SH signal ($I_{2\omega}$) generated by the nanoantenna was filtered by both a short-pass filter (SPF) and a band-pass filter (BPF) and then monitored by an electron-multiplying charge-coupled device (EMCCD).

S6 Second-harmonic signal and transmission signal

When the CW and femtosecond lasers captured a single QD in the nanoantenna, a series of sharp nonlinear spikes were detected in the SH signal as well as the transmitted pump signal. As the QD moved from the bottom of the potential well to the top of the barrier, the improvement in the electric field was computed to be 1.8, 1.5, and 1.3 for antenna with gaps of 5, 8, and 10 nm,

respectively. Since the SH signal is proportional to the square of the electric field, the enhancement in the SH signal was expected to be 3.24, 2.25, and 1.69 for the three gap sizes, respectively. The measured average intensity increase in the SH signal was 3.26, 2.0, and 1.85, which agreed with those obtained from the simulation (Figure S4A-S4C). In the transmission signal, synchronous negative spikes were observed, which was believed to be due to the QD blocking of the nanometer size gap (Figure S4D–S4F).

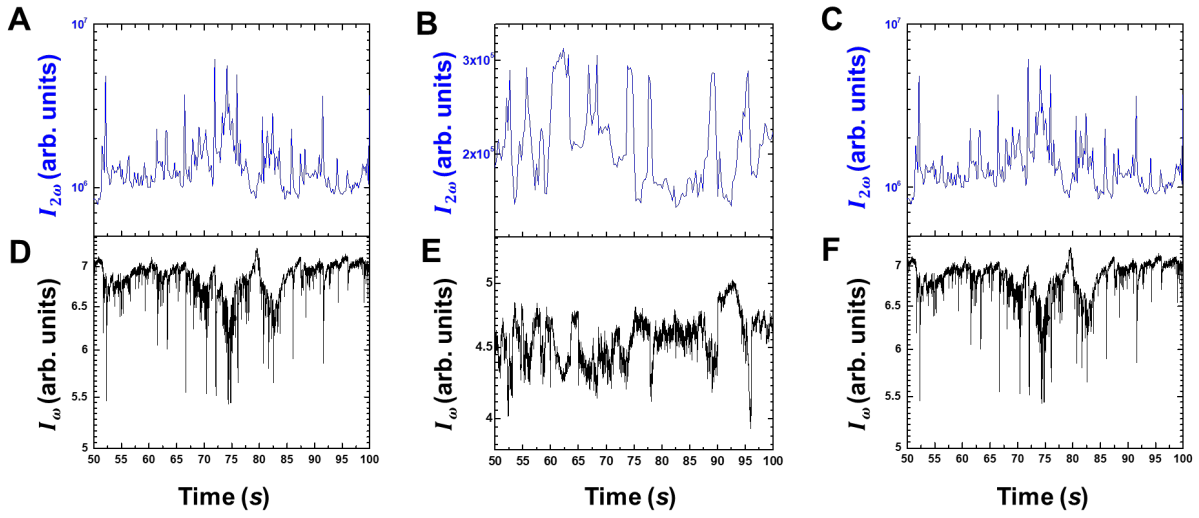

Figure S4: Monitoring the QD hopping. Time traces of the SH intensity ($I_{2\omega}$) and transmitted pump intensity (I_{ω}). The integration time for I_{ω} and $I_{2\omega}$ detection were 2 and 200 ms, respectively. Signals shown in (A) and (D) for the 5-nm-gap antenna, (B) and (E) for the 8-nm-gap antenna, and (C) and (F) for the 10-nm-gap antenna, were recorded simultaneously. At the instant the QD crossed the barrier, a negative spike in $I_{2\omega}$ and a positive peak in I_{ω} were generated simultaneously.

S7 Determining the barrier height that maximizes the hopping rate

Our optical trapping system corresponded to an overdamped regime, as described in Supplementary Material S1. Since the characteristic frequencies (ω_0, ω_b) and barrier height (U_b) were proportional to the same parameter P_{CW}, we can define the following relationships using constant coefficients c_0, c_b, and c_U.

$$\omega_0(U_b) = c_0 \times P_{CW}. \quad \text{(S17)}$$

$$\omega_b(U_b) = c_b \times P_{CW}. \quad \text{(S18)}$$

$$U_b = c_U \times P_{CW}. \quad \text{(S19)}$$

We substituted Equations S17-S19 into Equation S15 to obtain

$$f_c'(U_b) = \left(\frac{1}{F^2}\right)\left(\frac{(c_0/c_U) \times U_b}{\pi}\right)\left(\frac{(c_b/c_U) \times U_b}{\gamma}\right) exp\left(-\frac{U_b}{k_B T}\right)$$

$$= \left(\frac{1}{F^2}\right)\left(\frac{c_0 c_b}{c_U^2}\right)\left(\frac{1}{\pi\gamma}\right) \times (U_b)^2 \, exp\left(-\frac{U_b}{k_B T}\right). \quad \text{(S20)}$$

The derivative of Equation S20 implies that the hopping rate is the maximum when $U_b = 2k_BT$, which is apparent in Figure S5.

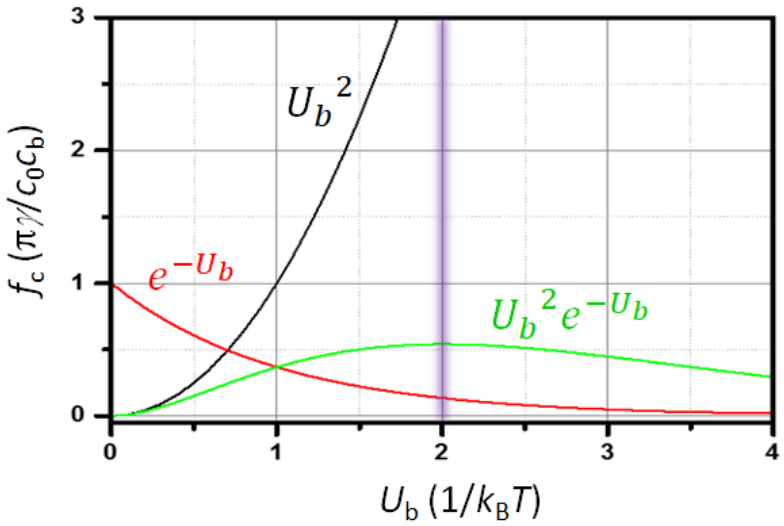

Figure S5: Roll-off frequency as a function of the central barrier height. The green line is the roll-off frequency and has the maximum at $U_b = 2k_BT$ (Purple-shaded region). Below $2k_BT$, the effect of U_b^2 term (black line) is dominant over that of e^{-U_b} term (red line), and vice versa.

S8 Air bubble formation in the nanoantenna

In our experimental setup, the CW trapping laser could deliver 70 mW power to a nanoantenna. We monitored the hopping characteristics at each P_{CW} while trapping the identical nanoparticle for a fair comparison. However, when the P_{CW} was at the threshold value of 53, 60, and 64 mW for groups G1, G2, and G3, respectively, the SH signal faded away (Figure S6A), while the transmittance was proportional to the P_{CW} (Figure S6B). At the same time, air bubbles appeared on the screen of the electron-multiplying charged-coupled device. The heat accumulation due to the intensive focusing of light generated an air bubble [12-15]. The bubble around the nanoantenna changed the refractive index from 1.33 (water) to 1 (air), and the resonant wavelength shifted to a shorter wavelength (Figure S6C). This hindered the field enhancement of the incident light and the generation of an SH signal.

Since the bubble disappeared as soon as the P_{CW} fell below the threshold P_{th}, it was considered to be composed of water steam rather than dissolved gas in water. Then, we can assume that the temperature of water T increased linearly from room temperature T_r to boiling point T_b as P_{CW} reached the threshold point.

$$T = T_r + \frac{T_b - T_r}{P_{th}} P_{CW}. \quad \text{(S21)}$$

The P_{CW} at the maximum hopping rate can be computed using the following equation that can be obtained by substituting Equation S19 and S21 into $U_b = 2k_BT$.

$$c_U P_{CW} = 2k_B \left(T_r + \frac{T_b - T_r}{P_{th}} P_{CW} \right). \quad \text{(S22)}$$

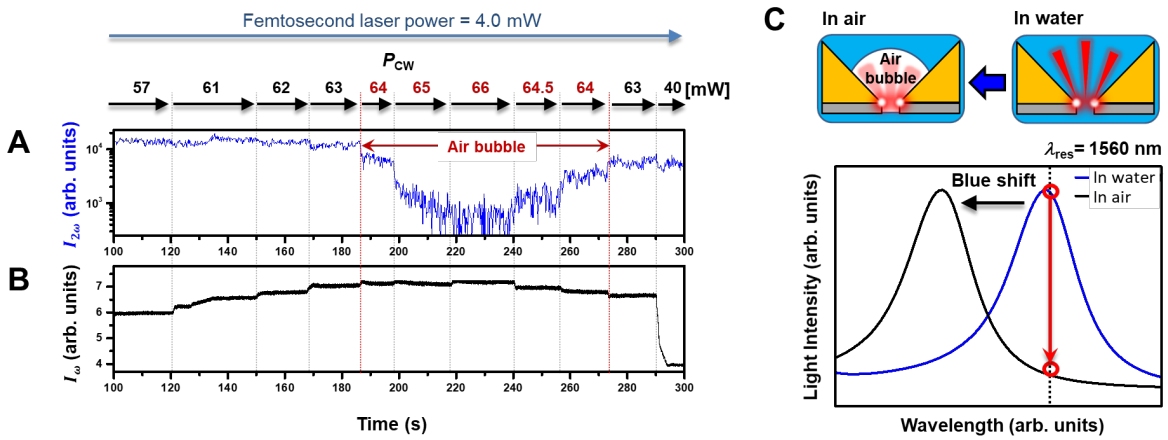

Figure S6: Air bubble formation phenomenon. Time traces of (A) SH intensity ($I_{2\omega}$) and (B) transmitted pump intensity (I_ω) signals for the 10-nm-gap antenna. The average power of the femtosecond laser was 4.0 mW, and the power of the CW laser was increased stepwise from 57 to 66 mW during the interval t = 100–240 s. At P_{CW} of 64 mW (t = 188 s), $I_{2\omega}$ started to decrease due to the formation of an air bubble, and it became very weak at 66 mW (t = 220 s). After t = 240 s, P_{CW} decreased from 66 to 40 mW, and the SH signal recovered to its original level at a P_{CW} value of 63 mW (t = 275 s). The difference between $I_{2\omega}$ at t = 180 s and $I_{2\omega}$ at t = 280 s with the same pump power (P_{CW} = 63 mW) was because of the presence of the trapped QD. (C) The change in the environmental refractive index from 1.3 (water) to 1 (air) moved the resonance wavelength of the nanoantenna to a shorter wavelength and weakened the electric field enhancement.

References

[1] S. J. Yoon, J. Lee, S. Han, et al., "Non-fluorescent nanoscopic monitoring of a single trapped nanoparticle via nonlinear point sources," *Nat. Commun.*, vol. 9, p. 2218, 2018.

[2] K. C. Neuman, and S. M. Block, "Optical trapping," *Rev. Sci. Instrum.*, vol. 75, pp. 2787-2809, 2004.

[3] H. A. Kramers, "Brownian motion in a field of force and the diffusion model of chemical reactions," *Physica*, vol. 7, pp. 284-304, 1940.

[4] P. Hanggi, "Escape from a metastable state," *J. Stat. Phys.*, vol. 42, pp. 105-148, 1986.

[5] P. Hänggi, P. Talkner, and M. Borkovec, "Reaction-rate theory: fifty years after Kramers," *Rev. Mod. Phys.*, vol. 62, pp. 251-341, 1990.

[6] V. I. Mel'nikov, "The Kramers problem: Fifty years of development," *Phys. Rep.*, vol. 209, pp. 1-71, 1991.

[7] R. Ferrando, R. Spadacini, and G. E. Tommei, "The Kramers problem: Fifty years of development," *Phys. Rev. A*, vol. 46, pp. R699-R702, 1992.

[8] R. Ferrando, R. Spadacini, and G. E. Tommei, "Kramers problem in periodic potentials: Jump rate and jump lengths," *Phys. Rev. E*, vol. 48, pp. 2437-2451, 1993.

[9] H. Brenner, "The slow motion of a sphere through a viscous fluid towards a plane surface," *Chem. Eng. Sci.*, vol. 16, pp. 242-251, 1961.

[10] J. Leach, H. Mushfique, S. Keen, et al., "Comparison of Faxén's correction for a microsphere translating or rotating near a surface," *Phys. Rev. E*, vol. 79, p. 026301, 2009.

[11] E. Schäffer, S. F. Nørrelykke, and J. Howard, "Surface forces and drag coefficients of microspheres near a plane surface measured with optical tweezers," *Langmuir*, vol. 23, pp. 3654-3665, 2007.

[12] Z. Fang, Y.-R. Zhen, O. Neumann, et al., "Evolution of light-induced vapor generation at a liquid-immersed metallic nanoparticle," *Nano Lett.*, vol. 13, pp. 1736-1742, 2013.

[13] O. Neumann, A. S. Urban, J. Day, S. Lal, P. Nordlander, and N. J. Halas, "Solar vapor generation enabled by nanoparticles," *ACS Nano*, vol. 7, pp. 42-49, 2013.

[14] G. Baffou, J. Polleux, H. Rigneault, and S. Monneret, "Super-heating and micro-bubble generation around plasmonic nanoparticles under cw illumination," *J. Phys. Chem. C*, vol. 118, pp. 4890-4898, 2014.

[15] A. Miniewicz, S. Bartkiewicz, H. Orlikowska, and K Dradrach, "Marangoni effect visualized in two-dimensions Optical tweezers for gas bubbles," *Sci. Rep.*, vol. 6, p. 34787, 2016.